FINAL REPORT

FOR CRADA NO. C-06-04

BETWEEN

BROOKHAVEN SCIENCE ASSOCIATES

AND

PHYSICAL OPTICS CORPORATION

Project Entitled: Instrument Development of Real Time Holographic Water Drop Size Measurement System

Brookhaven PI: Stephen R. Springston

Submitted by: Michael J. Furey
Manager, Research Partnerships
Brookhaven National Laboratory

DISCLAIMER

FINAL REPORT

FOR CRADA NO. C-06-04

BETWEEN

BROOKHAVEN SCIENCE ASSOCIATES

AND

PHYSICAL OPTICS CORPORATION

Project Entitled: Instrument Development of Real Time Holographic Water Drop Size Measurement System

Brookhaven PI: Stephen Springston

Submitted by: Michael J. Furey
Manager, Research Partnerships
Brookhaven National Laboratory

DISCLAIMER

BNL-91099-2007

Environmental Sciences Dept./Atmospheric Sciences Div.

Stephen R. Springston
Building 815E
P.O. Box 5000
Upton, NY 11973-5000
Phone (631) 344-4477
Fax (631) 344-2887
srs@bnl.gov

BROOKHAVEN NATIONAL LABORATORY

managed by Brookhaven Science Associates
for the U.S. Department of Energy

www.bnl.gov

MEMO

Date: February 7, 2007

To: M.J. Furey

From: Stephen R. Springston

Subject: CRADA No. BNL-C-06-04 between BNL and Physical Optics Corporation

Physical Optics Corporation (POC) was unaware of the requirement to produce a final abstract. With their input, I have drafted this response.

1) Accomplishments: BNL participated with multiple correspondences with POC on the design considerations of an airborne instrument. A pod for external deployment of the POC unit on the DOE Research Aircraft Facility (RAF), an instrumented, Grumman G-1 aircraft was loaned to POC. BNL proposed evaluation flight tests between the POC unit and the BNL Cloud Aerosol Probe Spectrometer (CAPS) as a reference method. BNL's involvement is described in the semi-annual report of POC to DOE.

2) Significant Problems: Because of unanticipated technical and engineering difficulties, POC was unable to fit their instrument into an aircraft pod. As a result they are now focusing on a ground-based version first.

3) Industry Benefits Realized: To be determined.

4) Laboratory Benefits Realized: A prototype laboratory version of the Real-Time Holographic Water Drop Size Measurement (WDSM) System has been constructed.

5) Recommended Follow-On Work: POC reports satisfactory progress in their semi-annual report. BNL is available for extension and/or expansion of the existing arrangement in order to provide assistance and evaluation of an airborne unit.

Real Time Holographic Water Drop Size Measurement System

Semi-Annual Report #2

Grant No. DE-FG02-04ER84042
Period of Performance: 07/11/05 to 07/10/07
Reporting Period: 02/11/06 to 07/10/06

Contractor:
Physical Optics Corporation
20600 Gramercy Place, Building 100
Torrance, CA 90501

Technical Monitor:
Ricky C. Petty
(301) 903-5548

Principal Investigator
Program Manager
Fedor Dimov, Ph.D.
(310) 320-3088

August 2006

TABLE OF CONTENTS

1.0 SUMMARY

In the second half year of the Real-Time Holographic Water Drop Size Measurement (WDSM) System project, Physical Optics Corporation (POC) designed optics for the system; continued developing a compact photothermoplastic (PTP) module; designed and assembled a WDSM module; worked closely with our consultant on fabricating a spray mechanism for laboratory WDSM testing; assembled a power-efficient laser light sheet subsystem to illuminate the object; and continued developing interface software and algorithms. In summary, the WDSM project is progressing as scheduled.

2.0 PROJECT STATUS

The project is proceeding according to the schedule in Figure 2-1.

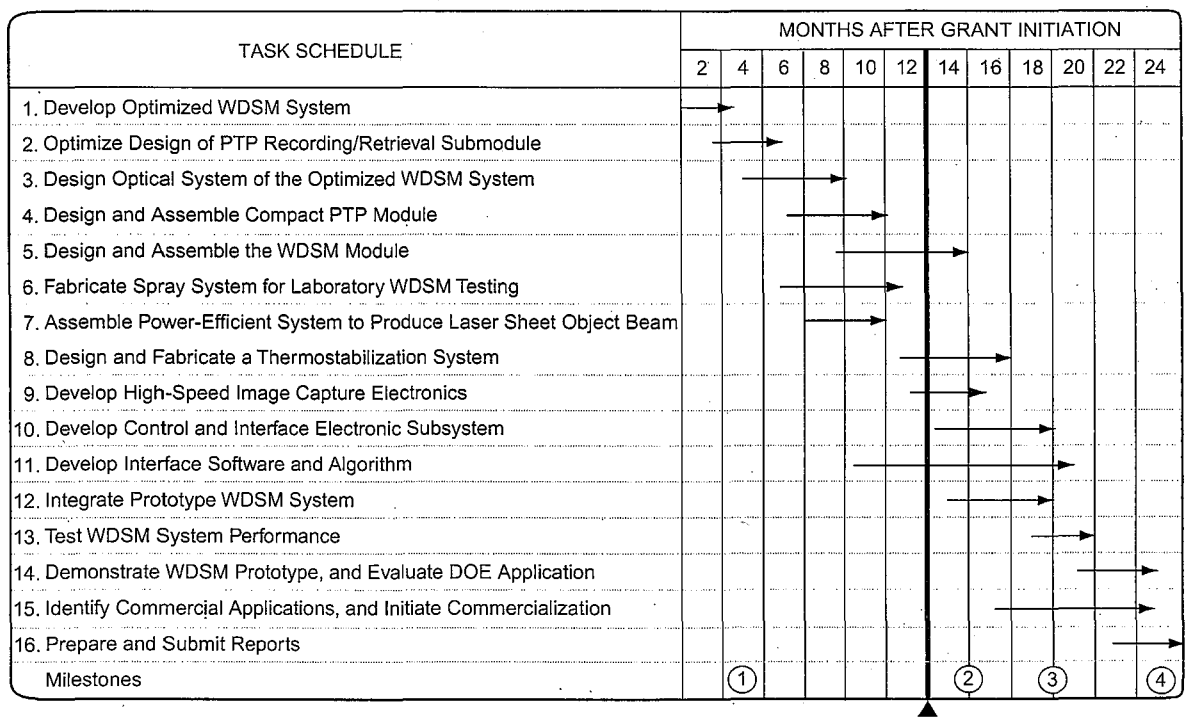

Milestone 1. Complete design of the optimized WDSM system
Milestone 2. Demonstration of WDSM module
Milestone 3. Integration of WDSM prototype
Milestone 4. Demonstration of functionality of the WDSM prototype.

Figure 2-1
Performance schedule.

By the end of the first half year of Phase II, POC had made the following progress toward developing the WDSM system:

- Determined Optimized WDSM System (Task 1)
- Optimized Design of PTP Recording/Retrieval Submodule (Task 2)
- Began designing Optics of the Optimized WDSM System (Task 3)
- Initiated Design and Assembly of Compact PTP Module (Task 4)
- Initiated Development of Control and Interface Electronic Subsystem (Task 10).

In the second half year we continued working on the tasks that were ongoing and started working on new tasks in accordance with the schedule. In brief, our work in this period was as follows:

- Continued designing Optics of the Optimized WDSM System (preliminary version complete; to be optimized in remainder of project) (Task 3)
- Continued Designing and Assembling Compact PTP Module (preliminary version complete; to be optimized in remainder of project) (Task 4)
- Designing and Assembling a WDSM Module (Task 5)
- Fabricating Spray Mechanism for Laboratory WDSM Testing (preliminary version complete; to be optimized in remainder of project) (Task 6)
- Assembled Power-Efficient Subsystem to Produce Laser Sheet Object Beam (preliminary version complete; to be optimized in remainder of project) (Task 7)
- Initiated Design and Fabrication of a Thermostabilization Subsystem (Task 8)
- Initiated Development of High-Speed Image Capture Electronics (Task 9)
- Initiated Development of Interface Software and Algorithm (Task 11).

3.0 DESIGN OF OPTICS OF THE OPTIMIZED WDSM SYSTEM (TASK 3)

First we designed optics optimized for an airborne WDSM system, taking into consideration weight, dimensions, power, heat, sampling, warm-up, operator dependence, and environmental conditions. Standard 19 in. rack slide-mountable boxes are preferred for easy removal, and maintenance of instrument and laser power supplies. Hermetically sealed aluminum enclosures and minimal weight/size/power are preferred. According to our subcontractor, Dr. Stephen R. Springston, Senior Research Scientist at the Atmospheric Sciences Division Brookhaven National Laboratory (BNL) in Upton, NY, it is better to enclose the optics for the airborne WDSM system inside a rigid and compact air pod.

To familiarize us with the air pod, Dr. Springston lent us a used one, which consists of a cylinder 6 in. in diameter and 24 in. long, with two hemispherical caps (see Figure 3-1). The front cap of the pod has a probing needle, which does not fit our WDSM application. Dr. Springston said we may custom-design a new front cap to accommodate the test requirements of our WDSM system. Figure 3-2 shows the electrical connection accessories inside the pod, and Figure 3-3 shows an example of how the pod is attached or mounted to the outside of a plane.

Figure 3-4 is a schematic of the optics designed by POC to be enclosed in the pod for the optimized airborne WDSM system. The collimated pulsed laser beam enters the optics via mirror 1, and is divided into p- and s-polarized beams by a polarizing beamsplitting cube (PBS). The s-polarized beam is then converted to a vertical narrow line source by the laser sheet generator, which consists of a pair of cylindrical lenses (CL 1 and CL 2) with a focal length of 150 mm and -7 mm, respectively. The laser sheet beam illuminates the water drops. A high-quality low-aberration imaging lens, (L3, focal length F = 55 mm), collects the 90° scattered light from the drops ("objects") and projects the light through the PIP film onto a CCD camera, which collects the image or fringes of the object as the CCD moves close to or away from the image plane. The selected magnification ratio is m = 8:1. The image plane can be calculated by $v = F(1+m) = 55(1+8) = 495$ mm, which is 495 mm from the lens or ~22 in. from the object ($u = v/m = 61.875$ mm, $v+u = 556.875$ mm = ~22 in.).

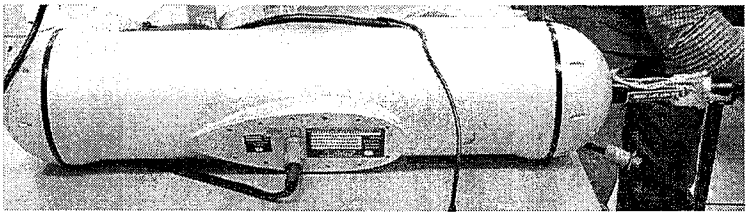

Figure 3-1
Pod to hold airborne WDSM system

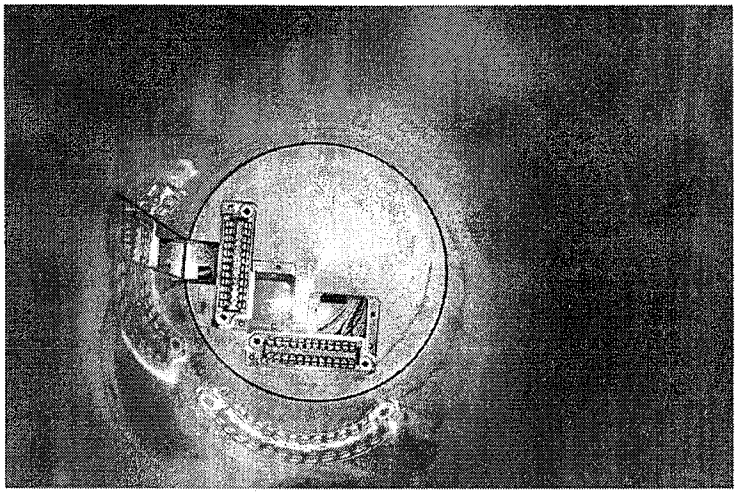

Figure 3-2
Electrical connection accessories inside the pod.

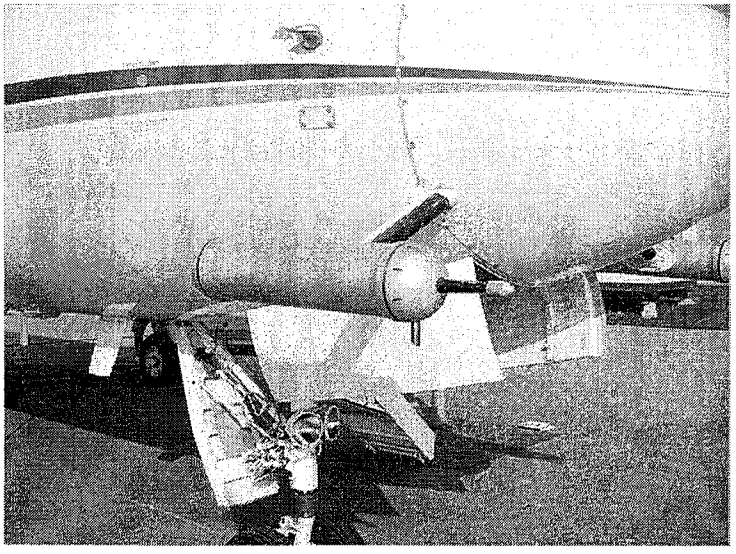

Figure 3-3
Pod attached to a plane.

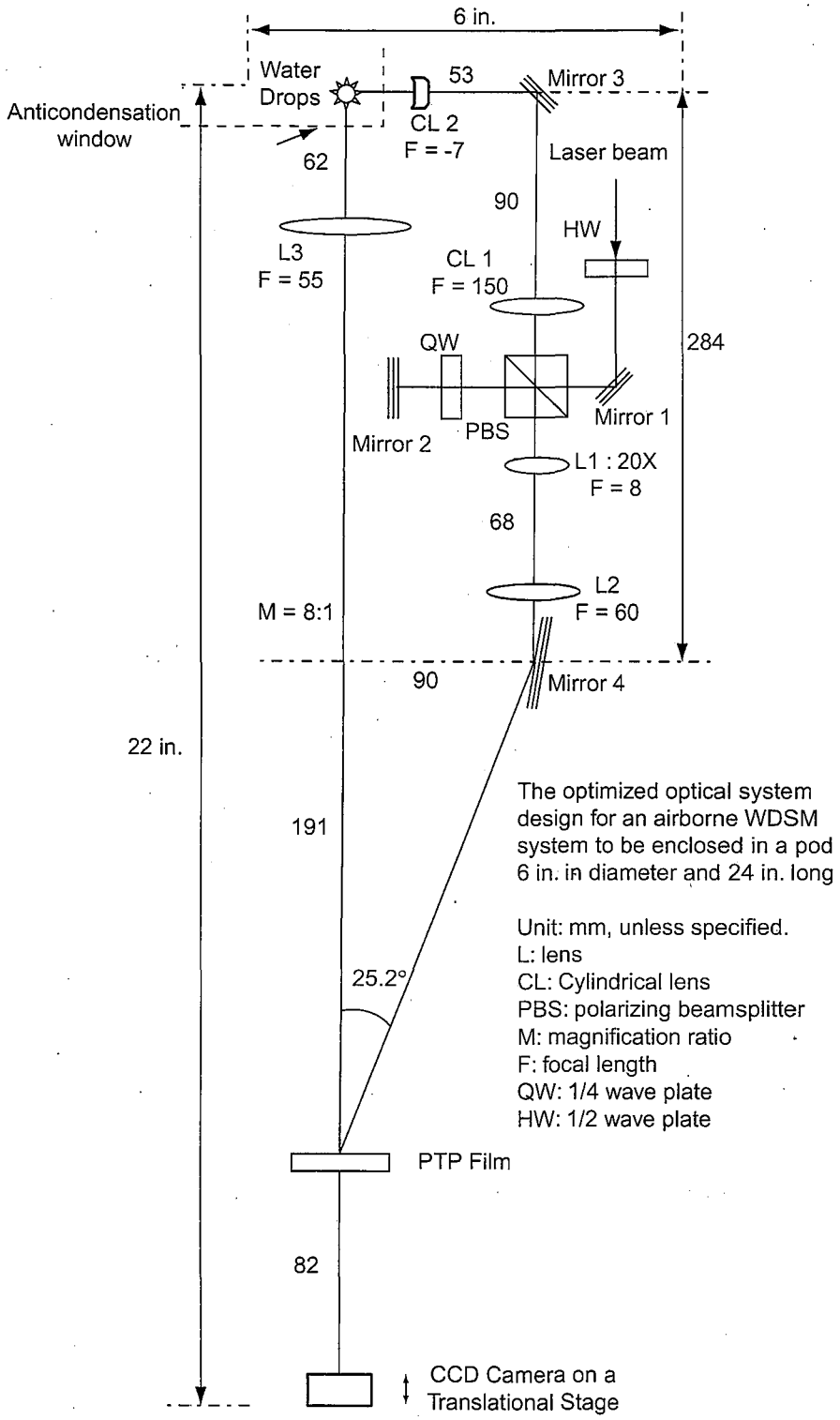

Figure 3-4
Optical system design of the optimized airborne WDSM system.

The p-polarized beam is converted to an s-polarized beam after it is reflected back by mirror 2 and passes twice through the quarter wave plate (QW). The s-polarized beam is then reflected by the PBS to the reference arm, and is expanded by a beam expander that consists of lens 1 (F = 8 mm) and lens 2 (F = 60 mm). A pinhole spatial filter at the confocal plane between the two lenses improves the beam quality, reducing the M square factor to ~1. The reference beam is reflected by mirror 4 and interferes with the object beam at an angle of 25.2° on the PTP film, which records a hologram of the object.

Since the short pulsed laser source, an ~10 ns Q-switched Nd:YAG laser with a second harmonic generator, has a coherence length of only ~5 mm, it is essential to adjust and optimize the position of mirror 2 along the optical axis so that the optical path length mismatch between the object and reference arms is minimized to within the range of the coherence length. The half wave plate (HW) before mirror 1 adjusts the energy ratio between the object and reference beams for optimized holographic recording. Mirror 3 folds the object beam to make the system more compact. The overall dimensions of the optics are <6 in. in diameter and ~22 in. in length, so it fits inside the 6 in. × 24 in. pod. The anticondensation window shown in Figure 3-4 will be adjusted to the pod design.

We have assembled a compact WDSM optics module based on the airborne design in Figure 3-4, and conducted some preliminary experiments and tests on glass beads in the laboratory, as summarized in Section 5.0.

In addition to the airborne WDSM system, we designed an optimized ground-based WDSM system. The optics will be enclosed in a 19 in. rack-mountable box (see Figure 3-5). This 19 in. rack box is 5.2 in. tall, and has an optical breadboard with 1/4 in. 20-thread mounting holes on 1 in. centers at the bottom; the 15.5 in. × 16 in. effective area is sufficient for mounting the optical components. The extensive series of quick connect subpanels includes a fiber connection, an electrical connection, a cooling fan, an AC power entry module, and blank panels. We have purchased a 19 in. rack box with no subpanels from Thorlabs, have started to assemble the optics, and will order subpanels for the electrical connection and AC power entry module as we progress.

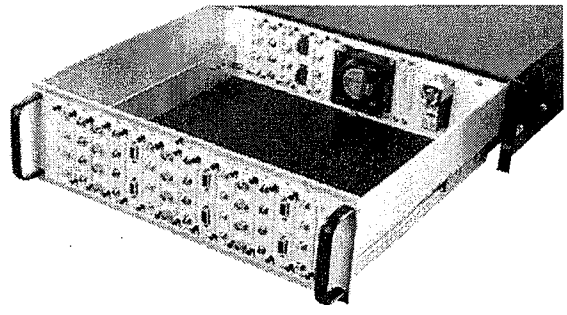

Figure 3-5
19 in. rack box [1].

Figure 3-6 is the schematic of the ground-based WDSM system. As seen, the optics, including the laser sheet generation optics, the object imaging optics, and the hologram recording and retrieval optics, is enclosed in a 19 in. rack box, represented by a square dotted box. The laser sheet generation optics, the object imaging optics, and the hologram recording optics are the same as in the airborne WDSM system (Figure 3-4). The retrieval arm optics consists of a compact CW laser, a shutter, and a beam expanding and filtering assembly that is the same as the one in the reference arm.

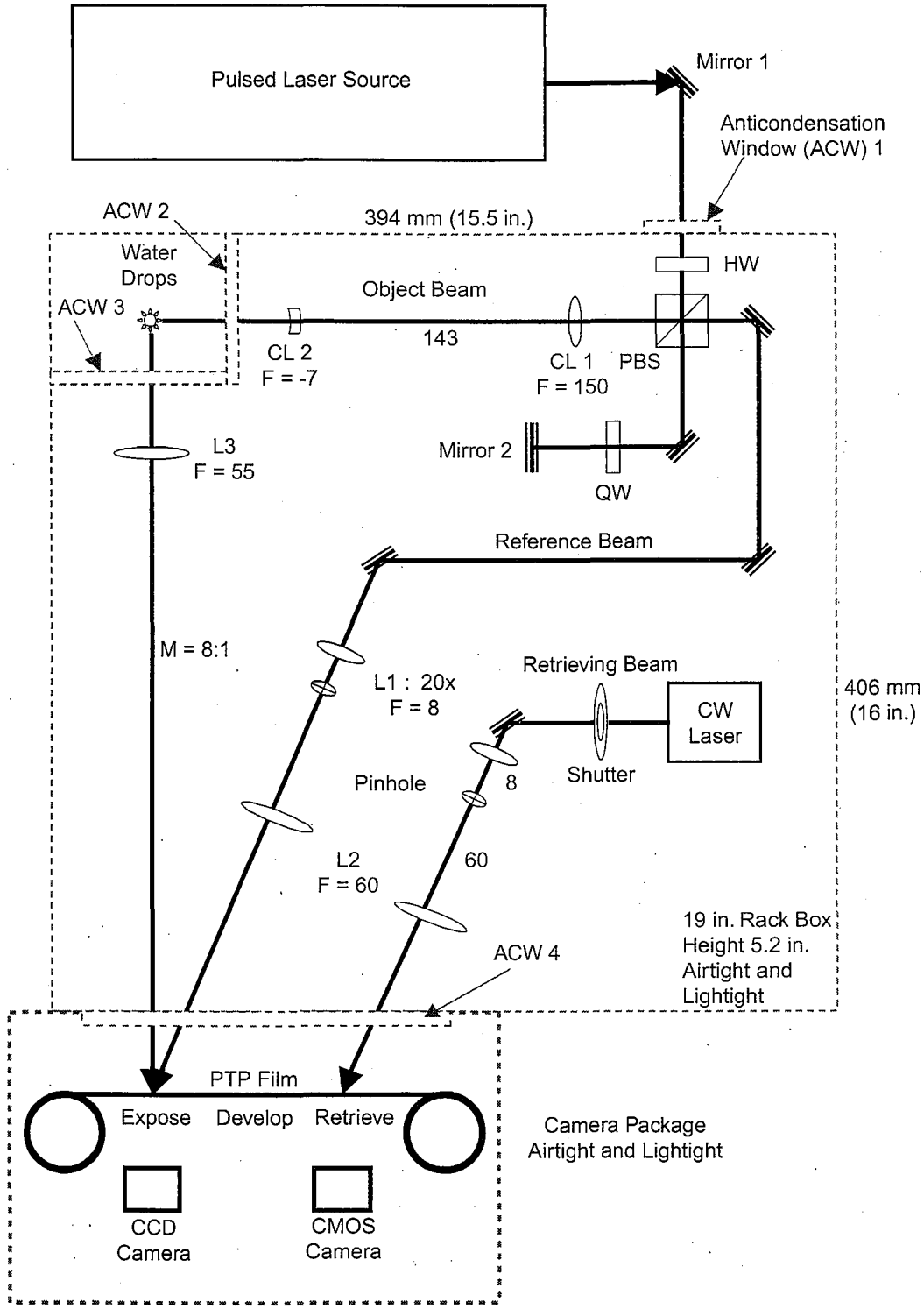

Figure 3-6
Design of an optimized ground-based WDSM system.

The pulsed laser beam for recording holographic images of water drops or fringes created by two bright spots enters the optics from the rear of the rack box. The PTP, CCD, and high-speed CMOS (or CCD) cameras are at the front of the rack box. Such a modular system design not only eases the fabrication and shipment of the ground-based WDSM system, but also increases flexibility in selection and upgrade of the pulsed laser source, PTP camera, and high-speed CMOS cameras, which are the components most dependent of high performance in the WDSM system.

For the compact CW laser in the retrieving arm, we plan to purchase an industrial-grade diode-pumped solid-state green laser such as the SCL-CW-532-100-9MM laser from Snake Creek Lasers, LLC (Figure 3-7).

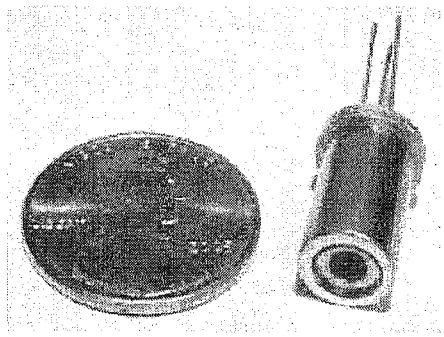

Figure 3-7
Snake Creek Lasers SCL-CW-532-100-9MM diode-pumped green laser [2].

This laser is the size of a paper clip and offers up to 100 mW linearly polarized output power with a high-quality (M square <1.1) TEM00 Gaussian spatial profile beam. The specifications of the laser follow:

Output Specifications:	**Input Specifications:**
Operating mode: Continuous wave	Voltage: <1.8 V
Output power: 0-100 mW	Current: <1200 mA
Output center wavelength: 532.43 nm	Electrical power: <2.5 W.
Polarization state: Linear	
Polarization contrast: >5:1	**Other Specifications:**
Full angle $1/e^2$ divergence: 7.5-8 mrad	CDRH class: III B
Beam diameter ($1/e^2$) at output window: 120 μm	Operating temperature: 10°C to 35°C without TEC
Output mode: Gaussian TEM_{00}	Warmup time: <1 min.
Beam quality: M^2 <1.1	Expected operating lifetime: >4,000 hr.
Residual 1064 and 808 nm leakage: <0.5%	
Peak-to-peak noise: <5%.	

4.0 DESIGN AND ASSEMBLY OF COMPACT PTP MODULE (TASK 4)

In the first semiannual report we included the results of research conducted with a Newport PTP camera, and described an existing PTP camera designed by the scientists of Moldova State University for recording common images on PTP film moving through a slit. Our contacts with

them led to the agreement that the Moldova team will design a PTP camera for hologram recording. POC initiated an CRDF (U.S. Civilian Research & Development Foundation) grant for Moldova State University. Here we include some preliminary results of this collaboration. No DOE money has been or will be spent on this development work, and no DOE-funded information is being provided to Moldava or anyone else outside the U.S.

4.1 PTP Structure, Thermoplastic and Recording Process Improvement for WDSM

A review of patents [3] has shown that to all appearances, the potential of one-layer (photoplastic) materials, combining in the same layer both photosensitive and thermoplastic properties, and double-layer (photothermoplastic) with individual functions of the photosensitive and thermoplastic layers, has been exhausted.

We believe that even the photosensitive layer, which is uniform in terms of chemical composition contains strata of different functions [4]. So, the photosensitive layer of the PTP medium for the WDSM will be designed to be multilayered. To produce this multilayered film, an adhesive layer is first deposited on the substrate, and then the conductive layer, or electrode is deposited. The next layer injects charge. Then a barrier layer is deposited, for which the heterostructure very often serves; then the transport layer and so on. Investigations [5] have shown that semiconducting weakly influences sensitometric parameters of the medium.

The visualizing layer (thermoplastic) will also be modified. The alteration of the type of polymer used, introduction of dopants in the last one, creation of one-layer and multilayer visualizing layers, and modifying the surface properties of thermoplastic allow us to optimize the regime of thermodevelopment by shifting the recording temperature diapason and potential of charging [6]. All this improves the parameters of the PTP medium to only a small degree. To meet the required parameters, the recording method itself is as important as the medium structure.

The recording system developed [6] is highly flexible in terms of generating electrostatic sensitivity, exposure, and heating of the PTPM. For every mode there is the optimal structure of medium and optimal materials. However, numerous modes of recording are possible on the same medium even with the same recording device [7], beginning from the classic, namely charging – exposure – heating for developing and ending with the traditional exposure for photography – charging – developing. For each the mode of recording on the same medium and with the same charging device, a different exposure curve is obtained.

The variety of constructions of charging devices is determined by the function of the apparatus. It succeeded in explaining the presence of the optimal charging regime for each charging device used in the apparatus for PTP recording and also to forecast the time (t) behavior of the surface potential $V_s(t)$ on PTPM when using charging device with known characteristics. So for the WDSM PTP camera designed, the parameters to provide maximal diffraction efficiency in the holograms recorded should be determined.

4.2 Photosensitive Layer Improvement

Investigation of the optical and photoelectrical properties has shown that varying the chalcogenide glass semiconductor (CGS) As_2S_3-As_2Se_3 composition allows us to tailor the properties of such films and to obtain layers satisfying any practical requirements. The basic

physical parameters of the CGS layers of different composition investigated are presented in Table 4-1.

Table 4-1. Basic Electrophysical Parameters of Investigated Layers of CGS

Samples		1	2	3	4	5
Chemical composition		As_2S_3	As-S-Se-Sn (0.13)	As_2S_3-As_2Se_3 (50:50)	As_2Se_3	As_2S_3-As_2Se_3 (30:70)
Measurements	Temperature (°C)	Values				
Average value of dark specific resistance (Ohm·cm)	(21±1)	$2\cdot10^{14}$	$7\cdot10^{14}$	$6\cdot10^{14}$	$3\cdot10^{12}$	$9\cdot10^{13}$
	(70±1)	$9\cdot10^{13}$	$1.3\cdot10^{14}$	$5\cdot10^{13}$	$7\cdot10^{11}$	$2\cdot10^{13}$
Maximum photosensitivity, nm		500	480	570	630	600
Photoresponse in maximum photosensitivity	(21±1)	4	30	11	13	15
	(70±1)	2	45	14	19	70
Power of the incident radiation in the maximum photosensitivity (W)		$1.4\cdot10^{-6}$	$8\cdot10^{-7}$	$6.6\cdot10^{-6}$	$1.6\cdot10^{-6}$	$9.1\cdot10^{-6}$
Sensitivity at maximum photoresponse (A/W)		cm $1.4\cdot10^{6}$	$1\cdot10^{5}$	$2\cdot10^{6}$	$2\cdot10^{5}$	$1\cdot10^{5}$

The bandgap decreases linearly when the composition is altered from $\Delta E = 2.4$ eV (As_2S_3) from 1.75 to 1.8 eV (As_2Se_3 Ohm·cm). The effective specific resistance of undoped layers had been changed from $2\cdot10^{14}$ Ohm·cm (As_2S_3) to $3\cdot10^{12}$ Ohm·cm. (As_2Se_3). Comparison of the results of investigation of optical and photoelectrical properties with drift mobility measurement shows that concentration of the local states in thin films of solid solution As_2S_3-As_2Se_3 drops with the growth of As_2S_3 content. And that drift mobility of the charge carrier decreases from 10^{-7} $cm^2/V\cdot s$ to 10^{-10} $cm^2/V\cdot s$ (As_2S_3). Because the processes of charge carrier transport in the layers of a solid solution As_2S_3-As_2Se_3 system are controlled by the sticking levels, depth increases with the growth of the As_2S_3 content in the layers.

On the basis of the thin layers of CGS obtained, two-layered PTP medium was created. An experimental study and theoretical calculations have shown that for the two-layered PTPM considered, the kinetics of the charging current correlates with the kinetics of the surface potential. The last one has allowed the potential on the thermoplastic layer to be controlled by means of a computer program in the process of recording, optimizing the recording process,

minimizing the effects of a strong electrical field, and, as a result, decreasing significantly the value of optical noise in the image obtained.

The kinetics of surface potential V_s when the photosensitive layer of As_2S_3 As_2Se_3 and solid solutions on their base implemented in PTP film are being charged, confirms the complicated character of the processes taking place under the influence of a corona device. With the growth of the last one, the maximum appears on the curves of $V_s(t)$. The subsequent lowering of V_s, we believe, is connected with the growth of a space charge in the deeper levels. The screening of the surface potential by this charge leads to the apparent decrease of the effective thickness of the layer. In this case, the surface potential V_s, which determines the light sensitivity of PTPM, is formed by the charge, accumulating on the surface and in the bulk of layer as well as between them. With the use of a simple model, we calculated the effective depth **b** of the charge bedding and its amount **N**.

So, for the layers of As_2Se_3 with a thickness d = 2.4 μm, the values **b** and **N** were b = 1.5 μm, $N = 2\times10^{17}$ cm^{-3}. For the layers consisting of solid solution $(As_2Se_3)_{0.7}(As_2S_3)_{0.3}$ (d = 3.0 μm) these values were 1.9 μm and 3×10^{17} cm^{-3} respectively and, at least, for an As_2S_3 layer with 2×10^{17} cm^{-3} thickness d = 2.2 μm, the corresponding values were b = 1.6 μm and $N = 7\times10^{17}$ cm^{-3}.

These values of the concentrations of the accumulated charge are in good agreement with the values of densities of localized states in these materials. The growth of illumination increases the field of predominance of the bedding of a compensating charge, which leads to a more pronounced maximum on the $V_s(t)$ curve. Such dependence is not observed at temperature growth up to 80°C, which means that effective depth of charge bedding is not changed in this case.

We have investigated a wide spectrum of possible applications of double-layered PTP media, including manufacturing a prototype for photothermoplastic recording. The results obtained indicate that PTP media developed can be successfully utilized in systems for optical information processing in coherent light and in holographic recording.

4.3 PTP Hardware Design for WDSM

As follows from the previous discussion, the Moldova team has already conducted significant work to adjust the parameters of the PTP camera and film for WDSM application. After the CRDF grant is approved, we plan a business trip to Moldova, funded under that grant, to clarify the issues related to the PTP camera and film. The researcher from Moldova will visit POC to continue the work on PTP camera design. No DOE will be provided to them; they will only be given specifications for the camera. As a result a modified PTP camera, described in first half-year report, and integrate it with the WDSM optical setup as shown in Figure 3-6.

5.0 DESIGN AND ASSEMBLY OF A WDSM MODULE (TASK 5)

Based on the optics design in Figure 3-4 for the optimized airborne WDSM system, we developed and assembled a compact breadboard WDSM optical module, which is shown in Figure 5-1. We designed the module to investigate the feasibility of fabricating a workable WDSM module that is compact enough to fit inside the pod. As seen from Figure 5-1, except for the Newport PTP camera, the optical module, which consists of optical components in the object

and reference arms, is very compact, occupying an area <6 in. across and 22 in. long, which is smaller than the pod. Keep in mind that the relatively large Newport PTP camera is the only PTP camera we have, and is being used temporarily in this assembly for testing the imaging performance of the module. We are working closely with the vendor on developing a new and much smaller PTP camera that will eventually be substituted for the Newport PTP camera.

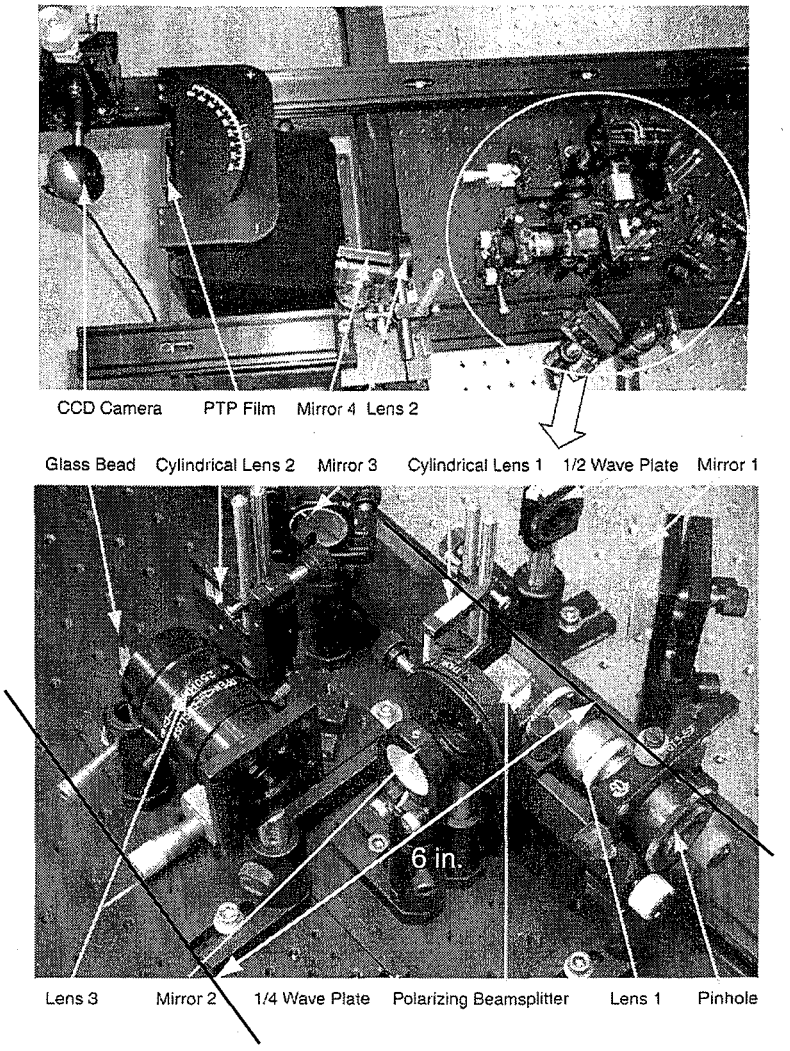

Figure 5-1
Compact breadboard WDSM optical module designed to fit inside the pod.
(The distance between two holes on the board is 1 in.)

We have conducted some preliminary experiments with the module. Figure 5-2 is a photo of a glass bead captured with the CCD camera (webcam) at the image plane. The two bright spots correspond to the intersecting points that were generated by the laser sheet at the front and rear surfaces of the glass bead. The bright vertical line below the two bright spots was caused by light scattering from the edge of the needle that held the glass bead. The CCD camera has an active area of 5 mm × 3 mm, from which we estimate that the distance between the two bright spots is ~0.8 mm, which corresponds to the image of an ~0.1 mm object, taking into account the

magnification ratio m = 8:1. The diameter of the glass bead we used in the experiment was actually ~0.1 mm, which agrees with our observations.

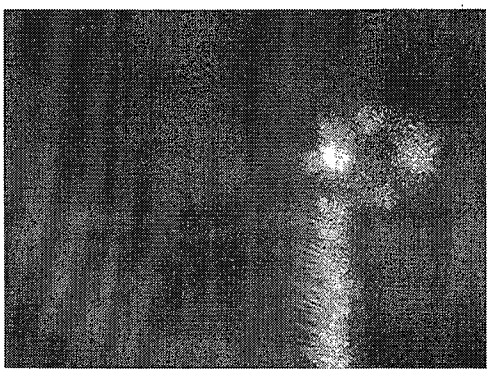

Figure 5-2
Glass bead.

Figure 5-3 shows the fringes from a glass bead, captured by the CCD camera at off-image plane. From the intensity distribution, we can calculate the diameter D of the glass bead based on the equation [8]

$$\eta \cdot D = \frac{\lambda}{\Delta\varphi} \quad , \tag{5-1}$$

where $\Delta\varphi$ is the angle between two neighboring maxima (or minima) of the intensity distribution (fringe). The factor η depends on the refractive index n of the drop and the observation angle θ as

$$\eta = \frac{\cos(\theta/2) + \dfrac{n\sin(\theta/2)}{\sqrt{1+n^2-2n\cos(\theta/2)}}}{2} \quad . \tag{5-2}$$

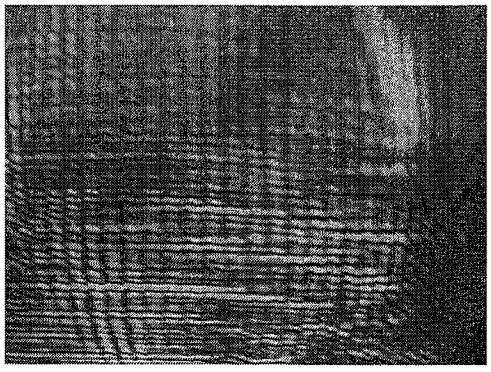

Figure 5-3
Fringes from the glass bead.

In our experiment, $\theta = 90°$, $n = 1.5$ (glass), and $\Delta\varphi = \sim 6.5$ mrad; therefore, we obtain $\eta = 0.8527$, and D =~0.096 mm, which is very close to the actual diameter of 0.1 mm.

We recorded holographic gratings on a PTP film with the Newport PTP camera. The recording area was ~1 in. in diameter. After the PTP film was recorded, it was developed and then retrieved with the same reference beam as was used in the recording. We then measured the power of the diffracted beam and calculated the diffraction efficiency of the holographic grating. The PTP film was then erased before being used to record another holographic grating at another reference/object power ratio and total exposure energy. Figure 5-4 shows the diffraction efficiency of holographic gratings recorded under varying exposure conditions (varying reference/object beam power ratio and total exposure energy). It appears that efficiency is optimal when the reference/object power ratio is ~1 and the total exposure energy is between 6 and 20 μJ. This experiment suggests that efficiency is optimal with an energy density of $\sim 10^{-5}$ J/cm^2 even though the sensitivity of the PTP film can reach 10^7 cm^2/J.

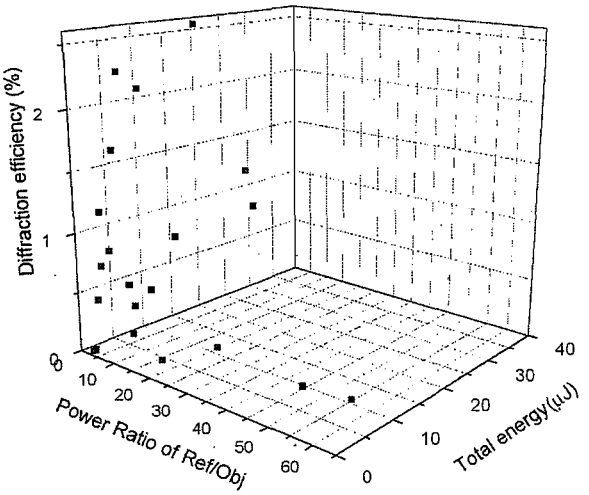

Figure 5-4
Diffraction efficiency of holographic gratings versus reference/object beam power ratio and total exposure energy.

6.0 FABRICATION OF SPRAY MECHANISM FOR WDSM LABORATORY TESTING (TASK 6)

We have worked closely with our subcontractor, Dr. Nels S. Laulainen, Senior Research Scientist in the Atmospheric Science Technical Group at Pacific Northwest National Laboratory (PNNL), on fabrication of a spray mechanism for WDSM laboratory testing. According to Dr. Laulainen's suggestion, a TSI Incorporated Model 3450 vibrating orifice aerosol generator (VOAG) (see Figure 6-1), can meet our requirements for WDSM laboratory testing. The VOAG produces solid or liquid aerosols from a wide variety of solutions. It creates aerosol particles that are uniform in size, density, shape, and surface characteristics. It is especially suited to controlled experiments for which airborne particle size must be known and within a narrow range. The specifications of the VOAG are listed in Table 6-1 [9].

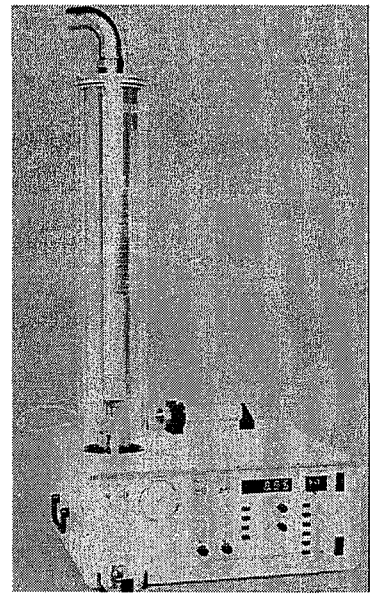

Figure 6-1
TSI Model 3450 vibrating orifice aerosol generator (VOAG) [9].

Table 6-1. VOAG Specifications

Mode of operation	Constant liquid feed rate through a vibrating orifice
Particle size range	1 to 200 μm
Initial droplet diameter	20 to 400 μm
Geometric standard deviation	<1.01
Particle type	Oil and solids soluble in water or alcohol
Particle generation rate	1,000 to 300,000 particles/s (depends on particle size)
Syringe pump	
Syringe ram speed	0.1×10^{-4} to 9.9×10^{-3} cm/sec
Flow rate	Selectable, 0.001 cm^3/min (10 cm^3 syringe) to 2.2 cm^3/min. (60 cm^3 syringe)
Syringe holders	Hold 10, 20, or 60 cm^3 syringes
Signal generator	
Frequency range	1 kHz to 1 MHz
Accuracy	±1% of full scale, ±1 digit
Amplitude of square wave	0 to 30 V, peak-to-peak
Physical specifications	
Cabinet size	44 cm × 37 cm × 20 cm (17.3 in. × 14.5 in. × 7.9 in.)
Weight: #	16 kg (35 lb.)
Drying: column height	60 cm (23.6 in.)
Drying: column material	Acrylic
Orifice material	Stainless steel
Electrical requirements	100/115/230/240 VAC, 50-60 Hz, 100 W maximum
Compressed air requirements	Up to 100 L/min. at 207 kPa (30 psig)

The VOAG vibrating orifice controls the breakup of a liquid jet, so it produces highly uniform droplets with a typical standard deviation of <1% of the mean droplet size. A syringe pump feeds a liquid solution through a small orifice at a predetermined rate (Figure 6-2). The volumetric flow remains constant. A piezoelectric ceramic driven by an oscillating voltage potential causes the orifice to vibrate at a constant frequency, producing a uniform droplet stream. The droplet stream is introduced into the center of a turbulent air jet, dispersing droplets and preventing coagulation. The dispersed droplets mix with a larger volume of clean, dry air, which evaporates any volatile portion of the droplets. The VOAG's integrated design makes it easy to start up and adjust. Liquid flow, dispersion air, dilution air, and oscillation frequency can be conveniently monitored and controlled from the front panel. Because the generation head, syringe pump, and signal generator are contained in one package, the VOAG collects all the data necessary to calculate final particle diameter.

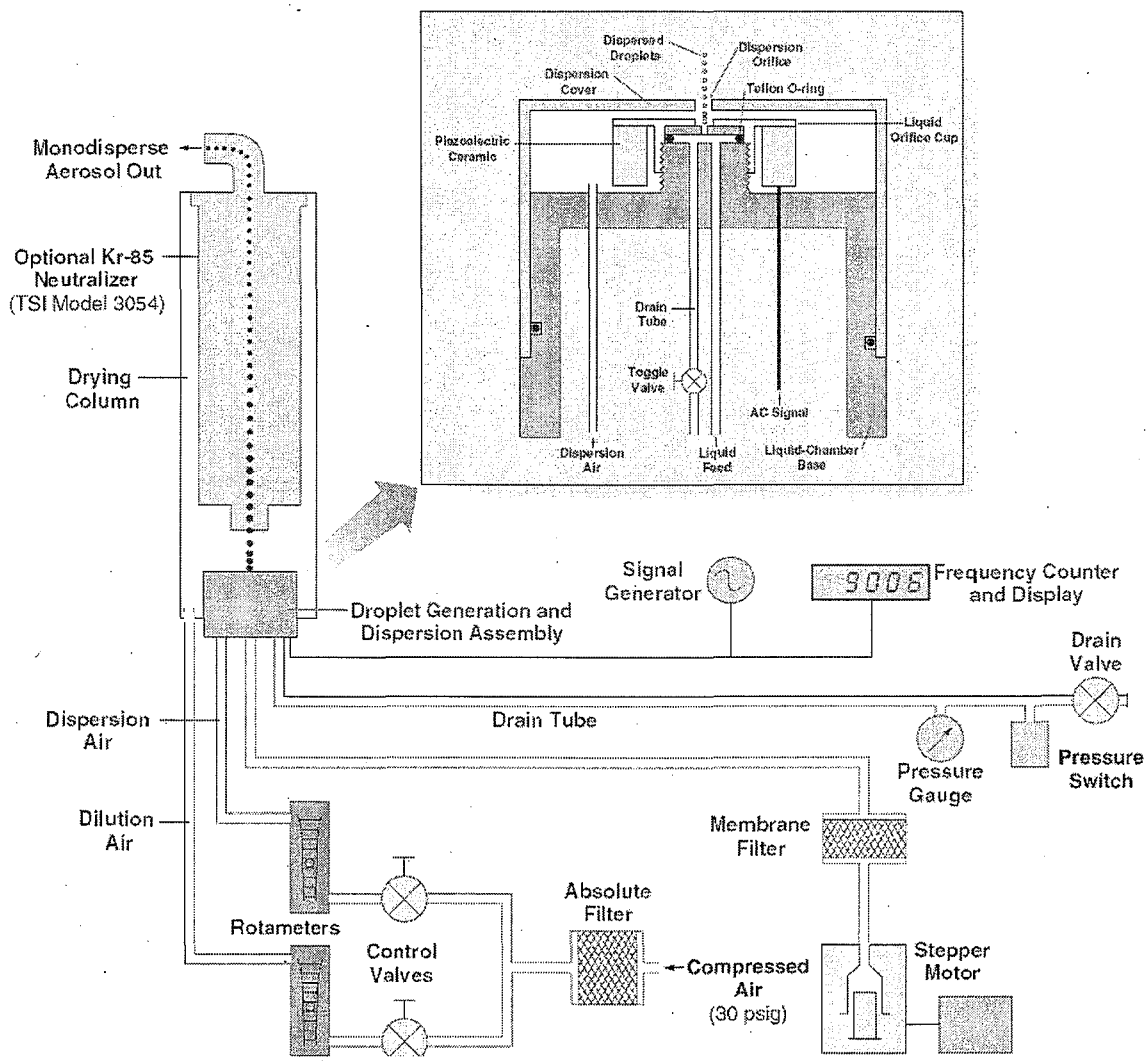

Figure 6-2
Schematic of VOAG spray system [9].

The VOAG can generate droplets from 20 to 400 μm in diameter. The solution used to generate the droplets determines evaporation and ultimate particle size. Because each disturbance cycle produces only one droplet, the precise size of the droplet can be calculated from the operating parameters. The two key parameters are liquid flow rate Q and oscillation frequency f. If a portion of the primary droplet is volatile, the final particle size depends on the volumetric concentration C, of the nonvolatile portion. From the Q, f, and C values, Eq. (6-1) calculates the final particle diameter [9]:

$$D_p = \left(\frac{6QC}{\pi f} \right)^{1/3} . \qquad (6\text{-}1)$$

By varying the liquid flow rate and oscillation frequency, the operator can generate a specific range of primary droplet sizes. Figure 6-3 shows a liquid droplet generated by the VOAG.

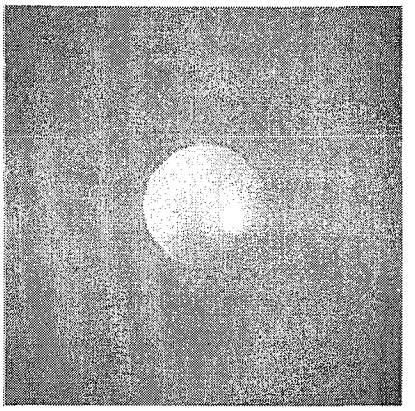

Figure 6-3
Typical droplet generated by the VOAG [9].

Dr. Laulainen has conducted spray experiments with a used VOAG spray system in his laboratory, and has recorded some preliminary data. He has agreed to lend us a VOAG spray system for WDSM laboratory testing. He plans to visit us in October and help us set up the system in our optical research laboratory, and train us in using it to generate water drops in varying concentrations and in sizes from 3 to 200 μm.

7.0 POWER-EFFICIENT ASSEMBLY FOR LASER SHEET OBJECT BEAM (TASK 7)

There are two types of layouts or assemblies for generating a laser sheet, as shown in Figures 7-1 and 7-2. In the configuration illustrated in Figure 7-1, the laser beam is horizontally compressed by two cylindrical lenses while maintaining its height. This layout is preferable if the required height of the laser sheet is comparable with the diameter of the laser source beam, and only the thickness of the laser sheet needs to be narrowed. Since the laser beam is compressed rather than expanded as in Figure 7-2, the laser power or energy required is much less. In other words, the Figure 7-1 layout is more power efficient than the Figure 7-2 layout. So far our WDSM system uses the Figure 7-1 layout because our laser source has a collimated beam diameter of ~5 mm,

which meets the requirement for the height of the laser sheet. The laser sheet assembly in our WDSM system consists of a positive cylindrical lens with a focal length F = 150 mm and an F = -7 mm negative cylindrical lens, and is designed to generate a laser sheet ~0.2 mm thick, which is appropriate for measuring water drops with diameters between 3 and 200 μm. The Figure 7-1 layout was implemented in the airborne WDSM system as shown above in Figure 5-1.

In Figure 7-2, the laser beam is horizontally compressed but vertically expanded by three cylindrical lenses. The Figure 7-2 layout requires a higher-energy (power) laser source, and is for applications such as particle imaging velocity measurement, for which a large laser sheet is required.

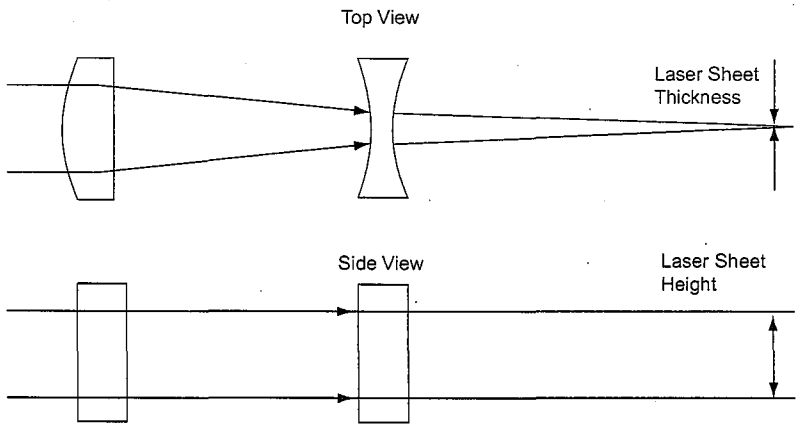

Figure 7-1
Generation of laser sheet horizontally compressed by two cylindrical lenses.

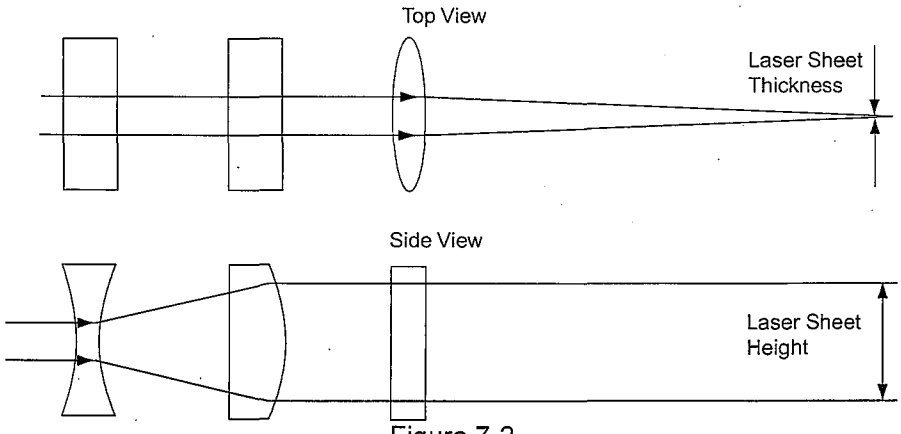

Figure 7-2
Generation of laser sheet vertically expanded by three cylindrical lenses.

The Figure 7-2 setup will be tested with a large volume with an increased number of water droplets to produce statistically significant results.

8.0 INITIAL DESIGN AND FABRICATION OF A THERMOSTABILIZATION SUBSYSTEM (TASK 8)

The optical windows of the WDSM sensor head will be designed and fabricated with anticondensation protection, as shown in Figure 8-1. High-temperature quartz heating cords (quartz-glass-covered wire elements) are wrapped around the windows for heating. Thermocouple sensors are attached to the windows to measure temperatures. A computer-aided temperature-control system will keep the sapphire windows at the right temperature to prevent condensation.

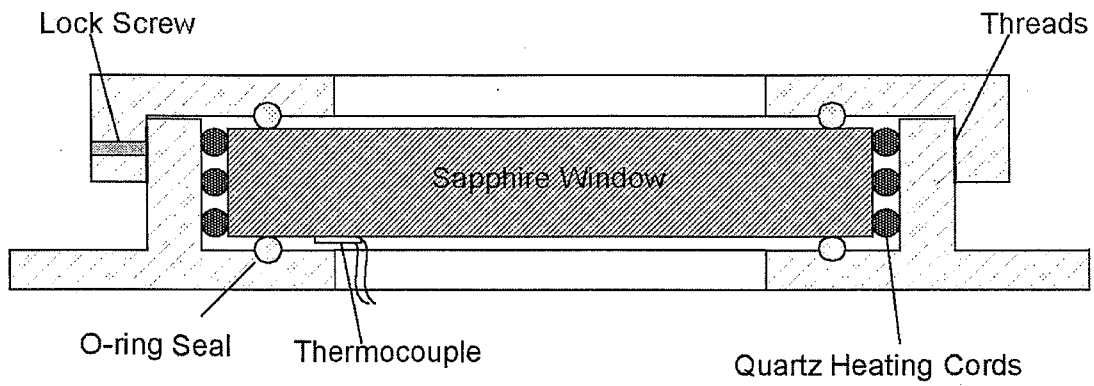

Figure 8-1
Design of the anticondensation window.

Sapphire was chosen for the window because it combines high transmission and high thermal conductivity with outstanding mechanical strength at high and low temperatures. Moreover, sapphire has excellent abrasion resistance and low temperature change index of refraction dn/dt and wavefront distortion. Because dn/dt is low, a temperature gradient across a window will cause negligible image blurring. This makes sapphire the material of choice for many stringent space and military applications such as high power laser windows.

The WDSM optical sensor head module will be hermetically sealed in a lightight, heatight and airtight enclosure, which will not contain any components that require circulating water cooling. To prevent ambient light from entering the lightight WDSM sensor head and causing the signal-to-noise ratio or modulation of the hologram to degrade, a green filter, which attenuates all spectra except for the 532 nm wavelength, will be mounted with each optical window.

Since the thermoplastic holographic recorder and PTP film are very sensitive to temperature, the enclosure will contain heaters and temperature controllers such as Kapton heaters (Figure 8-2), which heat up to 200°C (maximum heating power: 8 W/cm^2), and Digi-Sense C-08491-08 flexible thermistor probes (Figure 8-3), which measure air temperature from 0°C to 70°C with an accuracy of ±0.1°C, to keep the internal temperature of the enclosure within an appropriate range. To prevent optical components from moving/being displaced during aircraft acceleration (takeoff) and deceleration (landing), all optical mounts will be securely locked with pins after the optics are aligned and calibrated.

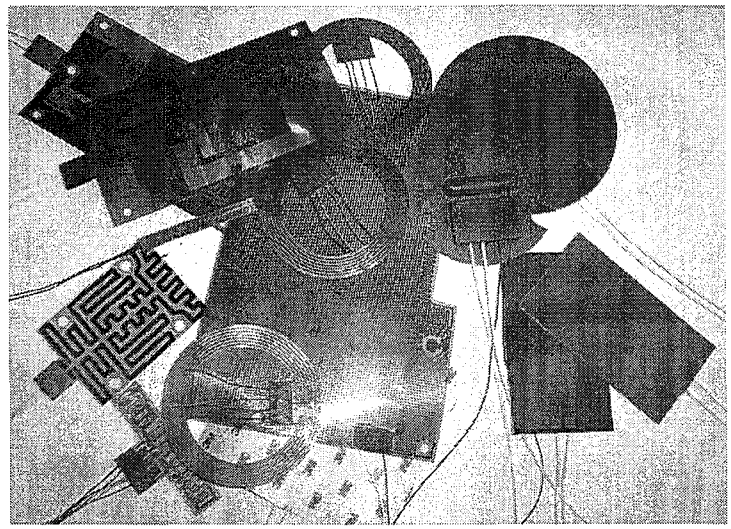

Figure 8-2
Kapton Heaters [10].

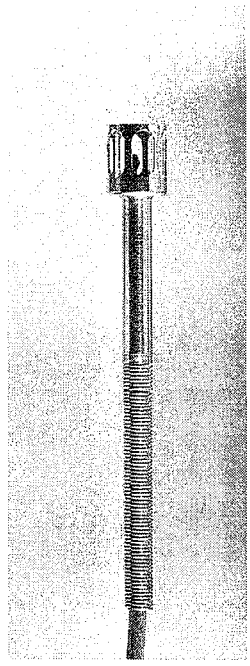

Figure 8-3
Digi-Sense C-08491-08 flexible thermistor [11].

9.0 HIGH-SPEED IMAGE CAPTURE ELECTRONICS (TASK 9)

The high-speed image capture electronics are for near-real-time capture and processing of the images or fringes of the water droplets in the process of holographic image retrieval. To this end, the CMOS or CCD camera must be able to capture and transfer at least a VGA resolution (640×480 pixel) 2D image in real time. We looked into some high-speed cameras, and believe the EmageWorks Pte Ltd Ranger CXMOS camera meets the needs of the WDSM system. The

Ranger CX is designed for high resolution and high-performance image processing, with a 2D pixel matrix and a row-parallel AD converter and processor architecture. The processor instruction set is optimized for image processing, with both local and global image processing operations implemented in hardware.

The Ranger CX camera is a smart CameraLink camera with frame rates of up to 30 kHz. It is compact, and connects to the PC through a standard CameraLink frame grabber in the PC and the CameraLink cable, as shown in Figure 9-1.

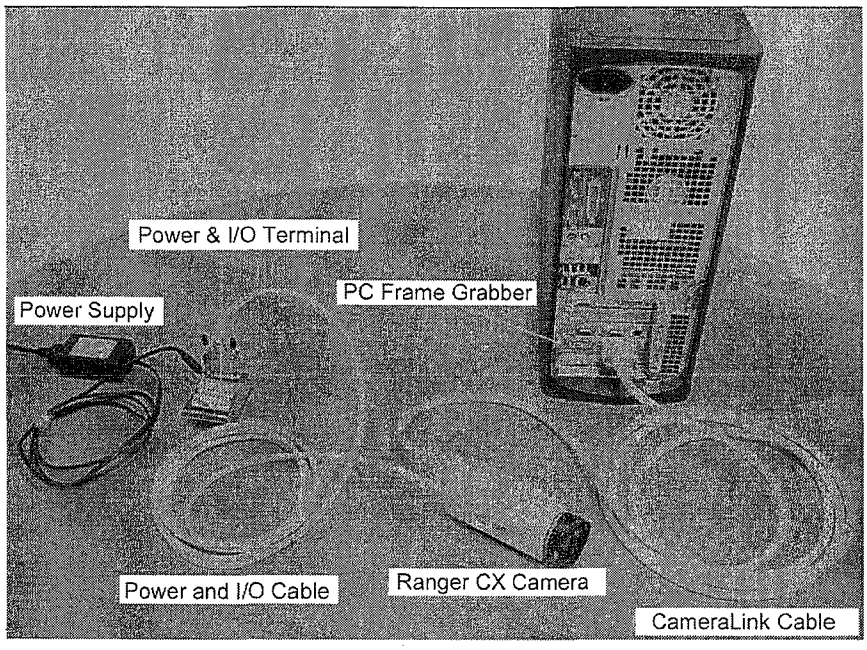

Figure 9-1
Compact Ranger CX camera, connected to a PC via a CameraLink card [12].

The standard CameraLink connection is used for high-speed data transfers from camera to frame grabber. The CameraLink channel also includes a low-speed asynchronous bidirectional serial communications channel (RS232 compatible) for camera control and software/firmware download. The camera can be synchronized with a PC and/or other cameras by TTL-level signals over either the power and I/O cable or the CameraLink cable. Over the power and I/O cable, five inputs and one output are available, while over the CameraLink cable, four inputs are available from the frame grabber board.

The Ranger CX data channel supports 1.1 Gbit/s in the CameraLink base configuration. The serial channel supports 115.2 bps for camera control and software/firmware download. Also, four inputs are available to the camera via the frame grabber board and CameraLink cable. The CameraLink frame grabber board and the CameraLink cable are standard products, also available from other vendors. To be able to utilize the full performance of the Ranger CX camera, the X64-CL dual or iPro frame grabber from Coreco Imaging [13] is recommended. In order to fully match the performance of the frame grabber, a 64 bit 66 MHz PCI slot is required in the PC.

The Ranger CX camera comes in three models, C55/C50/C40. The difference among them is the size of the sensor. C40 has a 512×512 pixel sensor area, while C50 and C55 have a 512×1536 pixel sensor area. The C55 is also equipped with an additional high-resolution row of 1×3072 pixels. In all other aspects the cameras are the same. Table 9-1 summarizes the sensor size and resolution for the C50 camera. Tables 9-2 and 9-3 give the CameraLink serial channel settings and electrical operating conditions, respectively.

Table 9-1. M12 Sensor Size and Resolution for the C50 Camera [12]

Parameter	Value
Pixel matrix size	4.864 × 14.592 mm
Pixel size	9.5 × 9.5 µm
Fill factor	60%
Horizontal resolution	1536 pixels per row
Vertical resolution	512 pixels per column
Optical center	Column 768, Row 227
Optics	1 in. C-mount

Table 9-2. CameraLink Serial Channel Settings [12]

Parameter	Value
Bit rate	115200 bps
Data bits	8
Stop bit	1
Parity	None
Flow control	None

Table 9-3. Electrical Operating Conditions [12]

Parameter	Min	Max	Unit
Power supply voltage	12	24	V
TTL input high (PIO connector)	2.0	5.75	V
TTL input low (PIO connector)	-0.5	0.8	V
TTL output high (PIO connector)	2.4	3.3	V
TTL output low (PIO connector)	0	0.4	V
Camera reset high	2.4	3.6	V
Camera reset low (active)	-0.3	0.8	V

Figure 9-2 plots the spectral response of the Ranger CX camera M12 sensor with a glass lid. The light charge collected in the Ranger CX camera can be digitized to 8 bit digital data representing gray scale values from 0 to 255. One AD unit represents one LSB in this 8 bit conversion. The unit in the spectral response graph below is (AD units per pixel)/(µJ/cm^2) which represents the digital gray value in a pixel over incident light energy. To obtain (AD units per pixel)/(incident light power) instead of energy, multiply the value by the integration time.

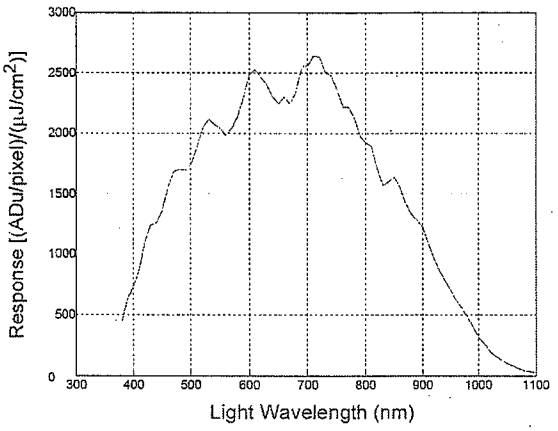

Figure 9-2
Spectral response with glass lid [12].

The peak sensitivity of 2640 (AD units per pixel)/(μJ/cm^2) is at 710 nm. The spectral response of the high-resolution line in a Ranger CX55 camera is approximately the same as the spectral response of the pixel matrix. The sensor response to a given amount of light incident on the sensor is calculated as follows.

1. Approximate the spectral distribution of your light source.
2. Map the shape of this distribution to the spectral curve of the sensor, and read (AD units per pixel)/(μJ/cm^2) for one or several wavelengths.
3. Determine the integration time for your application.
4. Translate the gray value per unit of energy from the curve in Figure 9-2 to the gray value per power by multiplying the value by the integration time.
5. Determine the incident light power on the sensor (irradiance, W/m^2) in your application.
6. Multiply this value by the sensitivity from step 4. The resulting sensor response is given as a digital gray value in AD units.

Example for retrieving the hologram: The CW laser source has an incident power of 0.01 mW/cm^2 or 0.1 W/m^2 (on the sensor area) at 532 nm.

The integration time is 10 ms.

At 532 nm the laser will give a sensitivity of ~2100 (AD units per pixel)/(μJ/cm^2).

The sensitivity will be $2100 \times 10^6 \times 10^{-4} \times (10 \times 10^{-3}) = 2100$ AD units/(W/m^2).

On the sensor, 0.1 W/m^2 will be incident. The response will be $2100 \times 0.1 = 210$ AD units per pixel.

10.0 DEVELOPMENT OF INTERFACE SOFTWARE AND ALGORITHM (TASK 11)

Figure 10-1 shows the control panels of the WDSM system control and analysis software module that was developed in LabVIEW. The software contains five modules. The "Measurement" module starts or stops the measurement of water drop size. The "Data Storage & Analysis" module analyzes and calculates the distribution of the water drop size, and saves and loads the data, including the calculated distribution curve of waterdrops, the retrieved images or fringes of waterdrops, etc. The "Measurement Results" module displays the images or fringes of measured water drops.

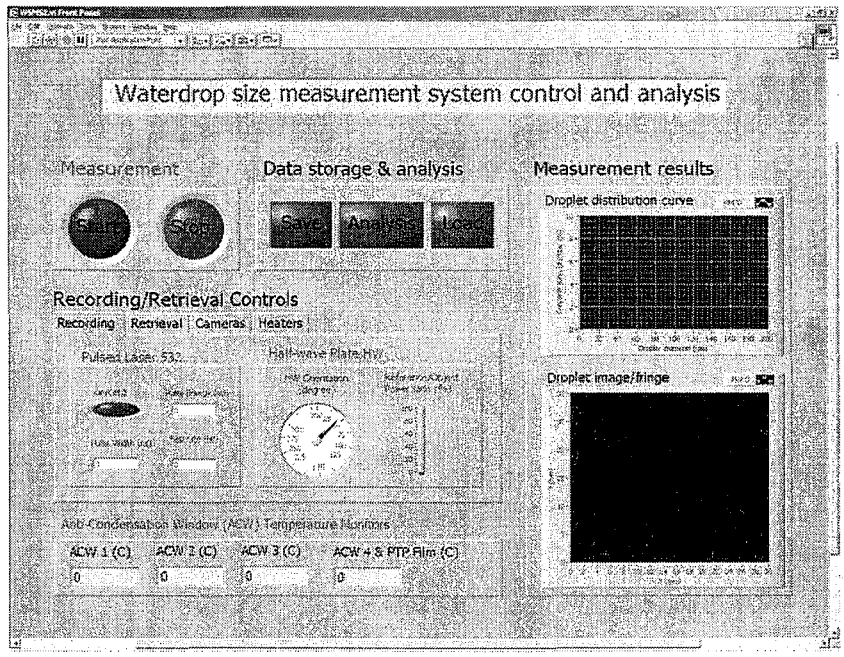

Figure 10-1
Hologram recording control panel of WDSM system.

The "Temperature Monitors" module acquires signals from the thermal sensors that monitor the temperatures at the optical windows and the PTP film, and displays the temperatures in real time. The analog signals from the thermal sensors are conditioned and then acquired via DAQ analog input (AI) channels.

The "Recording/Retrieval Controls" module initializes the device address of the DAQ board and the channel numbers of the AO and AI channels to be used. It also sets the address and the channel number of the IMAG board, and configures the RS323 serial ports for the control of the lasers. The "Lasers" subcontrol panel contains two subcontrols: one can turn the CW laser on/off and set its power, and the other can turn the pulsed laser on/off and set its pulse energy, duration, and repetition rate.

The "Retrieval Control" subpanel contains two subcontrol panels, one for the CW laser source, the other for the shutter, as shown in Figure 10-2. The "Cameras" subpanel contains two subcontrol panels, one for the CMOS camera, the other for the PTP film camera, as shown in

Figure 10-3. Figure 10-4 shows the subcontrol panels for the heaters. The control signals are delivered to the heaters via DAQ analog output (AO) channels.

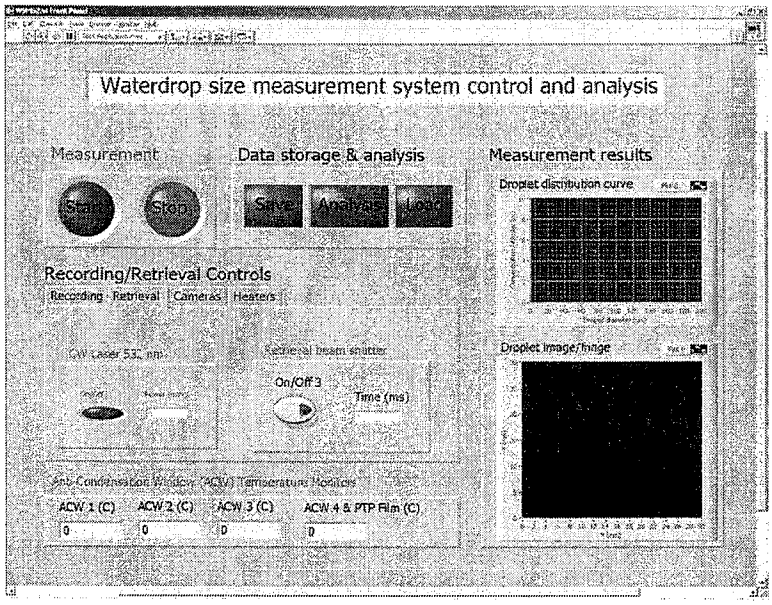

Figure 10-2
Retrieval control.

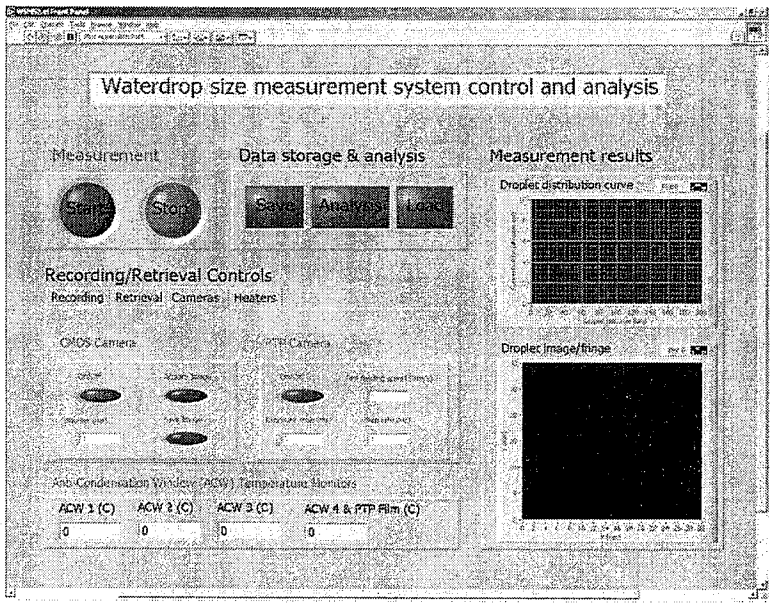

Figure 10-3
Camera control.

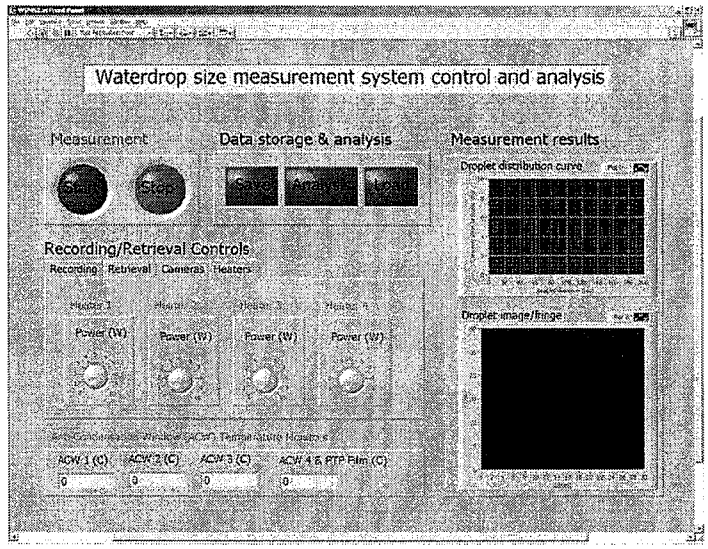

Figure 10-4
Heater control.

11.0 Future Work

During the next half year POC plans to finish the design of the ground-based WDSM system. The thermostablization system will be developed, as will the PTP camera. The development of the interface will continue. The computer interface and software will be integrated with the hardware, and the WDSM system will be tested with the use of a water droplet simulator provided by a DOE subcontractor. The analysis of the results of these tests should lead to the optimization of the WDSM during the first six months of the second year of Phase II for future implementation in airborne water droplet measurements. Commercial applications of the WDSM will be identified, and commercialization WDSM initiated.

12.0 REFERENCES

1. www.Thorlabs.com.
2. http://www.snakecreeklasers.com/documents/SpecSCLCW532-9.0mm.pdf.
3. L.M. Panasiuk, S.I. Kovtunenko, I.V. Ciapurin, Dep. VINITI, no. 1123-89.
4. R. Shaffert, *Electrophotographia*, M. Mir, p. 217, 1968.
5. L.M. Panasiuk, A.A. Muzalevskii, L.I. Pogorel'skii, et al., Zhurnal nauchnoi i priklad. foto- kinematografii, T. 30, n. 2, p.89, 1985.
6. L.M. Panasiuk and S.I. Kovtunenko, Zhurnal nauchnoi i priklad. foto- kinematografii, T. 33, n. 4, p.307, 1988.
7. L.M. Panasiuk, Abstracts of Report, *Intern. Congress on Photographic Science*, Beijing, China, p. 634, 1990.
8. K.H. Hesselbacher, K. Anders, and A. Frohn, "Experimental Investigation of Gaussian Beam Effect on the Accuracy of a Droplet Sizing Method," *Applied Optics*, vol. 30, p. 4930, 1991.
9. http://www.tsi.com/Product.aspx?Pid=58.
10. http://www.heat-insulation.com/Eng/jianjie.htm.
11. http://www.coleparmer.com/catalog/product_view.asp?sku=0849108&pfx=C.
12. www.emageworks.com.
13. http://www.coreco.com/.